Title

Detection of localized changes in the metabolism of hyperpolarized gluconeogenic precursors 13C-lactate and 13C-pyruvate in kidney and liver

Journal

Magnetic Resonance in Medicine, 77(4)

ISSN

0740-3194

Authors

von Morze, Cornelius
Chang, Gene-Yuan
Larson, Peder EZ
et al.

Publication Date

2017-04-01

DOI

10.1002/mrm.26245

Peer reviewed

HHS Public Access

Author manuscript

Magn Reson Med. Author manuscript; available in PMC 2018 April 01.

Published in final edited form as:

Magn Reson Med. 2017 April ; 77(4): 1429–1437. doi:10.1002/mrm.26245.

Detection of Localized Changes in the Metabolism of Hyperpolarized Gluconeogenic Precursors ^{13}C-Lactate and ^{13}C-Pyruvate in Kidney and Liver

Cornelius von Morze[1,*], **Gene-Yuan Chang**[2], **Peder E.Z. Larson**[1], **Hong Shang**[1], **Prasanna K.R. Allu**[2], **Robert A. Bok**[1], **Jason C. Crane**[1], **Marram P. Olson**[1], **Chou T. Tan**[3], **Irene Marco-Rius**[1], **Sarah J. Nelson**[1], **John Kurhanewicz**[1], **David Pearce**[2,*], and **Daniel B. Vigneron**[1]

[1]Department of Radiology and Biomedical Imaging, University of California, San Francisco, California, USA

[2]Division of Nephrology, Department of Medicine, University of California, San Francisco, California, USA

[3]ISOTEC Stable Isotopes Division, Sigma-Aldrich, Miamisburg, Ohio

Abstract

Purpose—The purpose of this study was to characterize tissue-specific alterations in metabolism of hyperpolarized (HP) gluconeogenic precursors ^{13}C-lactate and ^{13}C-pyruvate by rat liver and kidneys under conditions of fasting or insulin-deprived diabetes.

Methods—Seven normal rats were studied by MR spectroscopic imaging of both HP ^{13}C-lactate and ^{13}C-pyruvate in both normal fed and 24 h fasting states, and seven additional rats were scanned after induction of diabetes by streptozotocin (STZ) with insulin withdrawal. Phosphoenolpyruvate carboxykinase (PEPCK) expression levels were also measured in liver and kidney tissues of the STZ-treated rats.

Results—Multiple sets of significant signal modulations were detected, with graded intensity in general between fasting and diabetic states. An approximate two-fold reduction in the ratio of ^{13}C-bicarbonate to total ^{13}C signal was observed in both organs in fasting. The ratio of HP lactate-to-alanine was markedly altered, ranging from a liver-specific 54% increase in fasting, to increases of 69% and 92% in liver and kidney, respectively, in diabetes. Diabetes resulted in a 40% increase in renal lactate signal. STZ resulted in 5.86-fold and 2.73-fold increases in PEPCK expression in liver and kidney, respectively.

Conclusion—MRI of HP ^{13}C gluconeogenic precursors may advance diabetes research by clarifying organ-specific roles in abnormal diabetic metabolism.

Keywords

dynamic nuclear polarization; gluconeogenesis; diabetes; fasting; streptozotocin

[*]Correspondence to: Cornelius von Morze, Ph.D., Department of Radiology and Biomedical Imaging, University of California, San Francisco, 1700 Fourth Street, Byers Hall Suite 102, San Francisco, CA 94158. cornelius.vonmorze@ucsf.edu and David Pearce, M.D., Division of Nephrology, Department of Medicine, University of California, San Francisco, 600 16th Street, Genentech Hall Room N272C, San Francisco, CA 94158. david.pearce@ucsf.edu. .

INTRODUCTION

Fasting induces profound shifts in hepatic metabolism, sustaining systemic cellular respiration in the absence of dietary input. Among these, the mammalian liver exports large quantities of glucose by means of glycogenolysis and gluconeogenesis (GCN), supported energetically by the oxidation of fatty acids released from adipose tissues. With increasing duration of fasting and concomitant depletion of glycogen stores, GCN becomes the dominant mechanism of glucose export. Although the liver is the primary gluconeogenic organ during normal fasting, the kidneys supply substantial additional capacity, exporting increasingly significant quantities of glucose in extended fasting as well as diabetic and/or acidotic states (1).

In addition to their key roles in other metabolic pathways, lactate and pyruvate serve as dominant glucose precursors for GCN. Lactate is generated largely in skeletal muscle as an end product of anaerobic glycolysis. Its redox partner pyruvate and decarboxylation product acetyl-CoA function as main biochemical hubs of carbohydrate, fatty acid, amino acid, and ketone body metabolism, providing common entry of these various energy sources into the Krebs cycle (2). While some tissues can fully oxidize lactate itself as an energy source (3), circulating lactate is also the primary gluconeogenic substrate for both liver and kidneys (i.e., completing the glucose-lactate or Cori cycle). Because lactate and pyruvate are both readily transported into liver and renal proximal tubule cells by means of monocarboxylate transporters and because pyruvate is the first intermediate formed by lactate during conversion to glucose (in a reversible oxidation step catalyzed by lactate dehydrogenase or LDH), both are effective primary gluconeogenic precursors (4).

Similarly, circulating alanine also released from muscle serves as a secondary hepatic precursor also proceeding through pyruvate (i.e., completing the glucose-alanine cycle) (2), by means of a reversible transamination reaction catalyzed by alanine transaminase (ALT). Apart from these two dominant cycles, several other molecules including glycerol liberated from triglyceride fat stores and amino acids other than alanine (e.g., glutamine, a significant renal precursor) derived from muscle catabolism also serve as important gluconeogenic precursors by means of distinct pathways.

Given the central roles of lactate and pyruvate in cellular metabolism, there is a great demand for noninvasive methods to monitor localized metabolic activity of these substrates in vivo. Concerning their role as glucose precursors, establishing the relative role of liver versus kidney in the aberrant GCN of diabetes mellitus is an important biological question that can be addressed using HP ^{13}C MR of these substrates. GCN is of central importance to the pathophysiology of diabetes mellitus, accounting heavily for its characteristic fasting hyperglycemia. The differential regulation of hepatic and renal components is thought to be important but is as of yet poorly understood, due at least in large part to limitations of current methodology for studying localized metabolic changes in vivo (5).

While there exist some potentially noninvasive methods for systemic investigations of GCN using isotopic tracers (e.g., D_2O method) (6), prior methods to obtain localized data have

been severely limited by their high degree of invasiveness and difficulty. For example, measurement of renal gluconeogenesis requires catheterization of the renal vein and lengthy isotopic experiments (7), both of which are impractical for routine clinical use, and extremely difficult if not impossible in small animals. By providing ~50,000-fold nuclear magnetic hyperpolarization of ^{13}C-labeled compounds, dissolution dynamic nuclear polarization (DNP) has transformative potential for localized yet noninvasive studies of key biochemical pathways by MR spectroscopic imaging (MRSI), based on safe endogenous molecular imaging probes (8,9). A recent *first-in-man* imaging study demonstrates the safety and feasibility of this approach for investigating human disease (10). The goal of this initial study was to investigate changes in the spectra of HP GCN precursors ^{13}C-lactate and ^{13}C-pyruvate in the liver and kidneys of fasted and diabetic rats in vivo.

Compared with HP ^{13}C-lactate (11,12), HP ^{13}C-pyruvate has been much more thoroughly studied as a primary tracer (9,13–16), although no prior study has compared hepatic and renal components of data obtained using any HP GCN precursor during fasting or diabetes. As noted above both lactate and pyruvate are effective precursors, but under normal conditions circulating lactate is dominant; therefore, lactate is advantageous in its resemblance to the in vivo situation. While supraphysiologic quantities of pyruvate have generally been used for HP ^{13}C-pyruvate studies, similar quantities of lactate are much closer to the normal physiologic range, due to the higher normal concentration of lactate in vivo. Moreover, GCN from lactate and pyruvate proceed along theoretically different pathways: while oxidation of lactate directly supplies the cytosol with stoichiometric reducing equivalents necessary for GCN, the pyruvate pathway relies on additional redox steps (i.e., interconversion of oxaloacetate and malate) to shuttle the required energy between cellular compartments. Therefore, some important differences exist in the handling of lactate and pyruvate for GCN, of which the handling of lactate is arguably more relevant to the situation in vivo because lactate is the dominant GCN precursor.

We studied the effect of fasting and streptozotocin (STZ)-induced diabetes on localized metabolism of both lactate and pyruvate as HP ^{13}C probes. In vivo metabolic imaging of HP ^{13}C-lactate and ^{13}C-pyruvate with localization to the liver and kidneys was conducted in rats in normal fed, fasted, and diabetic states, using specialized ^{13}C MRSI acquisition techniques.

METHODS

Background on Methods for Probing Pathways of Glucose Recycling Using HP ^{13}C-Lactate and ^{13}C-pyruvate

The major pathways of glucose recycling are illustrated in Figure 1, with possible fates of a $^{13}C_1$ label in lactate or pyruvate indicated. Labeling either HP probe at this position facilitates tracking HP signals of both the original substrate and metabolic products [1-^{13}C]pyruvate, [1-^{13}C]lactate, and [1-^{13}C]alanine, and potentially also [^{13}C]bicarbonate. The observed interconversion of HP pyruvate and lactate signals has been shown to reflect largely an exchange of the HP label with the endogenous pools, as opposed to a true net metabolic flux, both in cells and in vivo (17,18). Similar considerations also apply to the interconversion of HP pyruvate and alanine signals.

Rapid demagnetization of the label by means of molecule-specific T_1 relaxation (e.g., with a decay constant of 45 s for aqueous [1-^{13}C]lactate at 3T) mostly precludes reliable detection of additional intermediates or products. Due to this rapid demagnetization, HP ^{13}C studies with metabolically active probes are generally limited to very rapid biochemical pathways. Early work in a perfused rat liver system established that intravascular lactate presented in high concentrations (e.g., 10 mM) to fasted liver is rapidly integrated into glucose and exported to the circulation (mean time of 80 s for conversion of lactate to blood glucose, with significant conversion occurring during the first 30 s) (4), suggesting that HP technology could be very suitable for studies of GCN. A recent study found that a substantial amount of ^{13}C label from injected HP [1-^{13}C]pyruvate enriches plasma glucose in rats on the time scale of HP experiments (19), indicating that injected HP materials are active along GCN pathways.

This rapid rate of GCN is not surprising given the very high rate of glucose usage in animals, particularly by the erythrocytes and the central nervous system. Because the entire plasma glucose pool is turned over on the time-scale of 1 h, a fasting rat must synthesize several milligrams of glucose per minute by means of GCN. Although HP ^{13}C-glucose derived from these HP substrates cannot be directly detected due to rapid demagnetization of the label (due to dipolar coupling with protons directly bonded to the labeled carbons), differential conversion of the label among the observable primary intermediates could indirectly reflect local bulk shifts of glucose metabolism between glucose breakdown and glucose formation.

Animal Experiments

Seven newly mature male Sprague Dawley rats (age = 8–12 weeks) underwent HP ^{13}C MRSI scans in both normal fed (standard rat chow) and fasted states, on separate days at approximately the same time of day (afternoon) separated by 4–14 days. Animals were fasted for 24 h but maintained free access to water. Seven additional newly mature male Sprague Dawley rats (same approximate age and weight) were scanned after selective ablation of beta cells by intraperitoneal injection of STZ, 60mg/kg (Sigma, St. Louis, MO), and confirmed diabetic by blood glucose level after 48 h. STZ is a widely used model of type 1 diabetes mellitus, which is characterized by an acute loss of endogenous insulin production due to destruction of beta cells, as opposed to type 2 diabetes mellitus, which is a much more common, chronic condition characterized by insulin resistance and beta cell dysfunction in varying proportions. After confirming the development of diabetes, each diabetic rat was scanned 24–36 h after withdrawal of insulin supplementation. Other than inducing diabetes by means of toxicity to beta cells, STZ can cause proteinuria by means of a direct toxic effect on the kidney, but no other aspects of renal function are known to be affected directly by STZ (20).

Before each scanning session, all rats were anesthetized by inhalational isoflurane (1.5%, gas flow rate 1 L/min) and a lateral tail vein catheter was implanted for introduction of HP ^{13}C media. The rat was positioned supine in a clinical 3 Tesla (T) MRI scanner (GE Healthcare, Waukesha, WI) inside a custom dual-tuned ^{13}C/^{1}H quadrature transceiver radiofrequency (RF) coil (l=8 cm; d=5 cm) on an embedded heated water pad. The animal

studies described in this manuscript were specifically approved by the University of California San Francisco Institutional Animal Care and Utilization Committee (UCSF IACUC, protocol #AN108035).

Dissolution DNP

The recent commercial availability of a pure acid form of ^{13}C-labeled lactate (Sigma), which like in the case of pyruvate exhibits greatly improved polarization by dissolution DNP over the sodium salt, has facilitated this work (12). At the same time, it also presented a unique challenge due to slight spectral contamination by dimeric and/or oligomeric forms of lactate found in these samples, due to the tendency of lactic acid to self-polymerize at high concentrations. This challenge was addressed by applying a novel pulse sequence strategy for spectrally selective suppression of these undesired spectral components as described below. For the lactate experiments, neat [1-^{13}C]-L-lactic acid, a solid at room temperature (melting point = 53 °C), was dissolved in a small quantity of distilled water (~10% by volume) and mixed with 15 mM trityl radical OX063 (Oxford Instruments, Tubney Woods, UK) and 1.0 mM Dotarem (Guerbet, Roissy, France) to improve the polarization. This addition of water reduced the concentration of labeled nuclei; therefore, the maximum achievable polarization, but was done to liquify the pure solid lactic acid. The alternative of heating the lactic acid was not chosen, because this could facilitate polymerization.

Detailed procedures for preparation of the [1-^{13}C]pyruvate samples have been described elsewhere. Each HP sample was polarized by DNP for ~1 h in a commercial Hypersense system operating at 3.35 T and 1.3 K (Oxford Instruments), and subsequently rapidly dissolved in 4.5 mL NaOH/Tris buffer, to bring the solution to the desired range of concentration and pH. Lactate attained polarization of ~26%, back-calculated to the time of dissolution (based on the measured T_1 = 45 s).

Hyperpolarized ^{13}C MRSI Studies

For each experiment, a rat underwent back-to-back HP ^{13}C MRSI scans with [1-^{13}C]lactate and [1-^{13}C]pyruvate, respectively. Rats were infused with ~2.5 mL HP solution (160 mM lactate or 80 mM pyruvate) over 12 s, followed by data acquisition. Both scans were designed to discriminate hepatic and renal components of HP tracer uptake and metabolism, but differed in the details of the MRI acquisition strategy. The experimental protocol is summarized graphically in Figure 2.

Lactate-derived signals were localized by three-dimensional (3D) MRSI with excitation of an axial slab covering both organs and double spin echo refocusing, with echo planar spectroscopic imaging (EPSI) for fast MRSI of a single 3D spectroscopic image (21). The acquisition parameters were: matrix= 6 × 6 × 16, FOV = 9 cm × 9 cm × 24 cm, 15 mm isotropic spatial resolution, variable flip angle over phase encodes to expend all magnetization (22), centric view ordering with acquisition starting at 30 s after start of infusion. Suppression of a confounding dimeric/oligomeric resonance in the vicinity of product [1-^{13}C]alanine was achieved by spectrally selective presaturation of this region of the NMR spectrum during the bolus infusion (23), exploiting the quenchable nature of HP

magnetization. The resonance had an amplitude of ~3% of the lactate peak, with similar T_1 (~43 s versus 45 s for lactate).

A train of 16 consecutive spectrally selective 90° maximum phase Shinnar-LeRoux RF pulses (24) with attendant spoiler gradient pulses was applied with repetition time 1 s, covering the entire duration of infusion. Each pulse had a duration of 20 ms and nominal suppression bandwidth of 125 Hz. Because suppression is practically limited by RF inhomogeneity, distributing the suppression pulses throughout the infusion ensures that each spin experiences at least one pulse that is very close to 90° as it passes near the center of the coil. A nonconfounded contaminant resonance also found in the spectrum served as a useful internal control. In a separate control experiment, the described presaturation approach was found to eliminate the signal of this nonconfounded resonance of similar intensity and T_1 relaxation time almost entirely. The described approach does not perfectly eliminate the contaminant signal but does provide a high degree of signal suppression.

For the pyruvate experiments, signals were localized to one of two adjacent axial slabs acquired sequentially, designated the liver and kidney slabs, respectively. Although each axial slab encompassed some additional tissues, based on prior experience with HP infusions the dominant contribution to each slab's signal at these time points was from the respective organ, with some small partial contamination by other tissues in the slice (25). Each rat was fully extended in the coil such that the liver and kidneys were well differentiated by adjacent axial slabs (thickness ≈ 17 mm, inter-slab gap = 3 mm), although a small amount of overlap is unavoidable. Each slab was excited repeatedly every 3 s by 20° excitation with double spin echo refocusing as above, over a period of 60 s starting 20 s after the start of infusion.

High bandwidth slab-selective excitation (>2kHz) ensured minimal chemical shift misregistration within the slabs. The rationale for coarser localization of the pyruvate signals was to maximize the likelihood of detecting low levels of additional intermediates such as oxaloacetate or aspartate, such as reported previously following infusions of HP [1-^{13}C]pyruvate (15,26). Based on the relatively low SNR of these reports, it is unlikely to be possible to further localize these signals, even by spatial signal averaging in postprocessing, which does not recover the full originally available SNR.

For anatomic reference, whole rat ^{1}H MRI images were also acquired using a coronal 3D balanced steady state free precession (bSSFP) acquisition (0.6 mm isotropic resolution, TE/TR = 2.5 ms/5.0 ms, scan time = 4 min, 55 s). The ^{1}H image data was reformatted for overlay of ^{13}C MRSI data.

Data Analysis

Metabolite peak areas localized to kidney and liver regions were tabulated for lactate, pyruvate, alanine, pyruvate-hydrate, and bicarbonate where applicable. For each comparison, magnitude spectra were integrated over a fixed range of offset frequencies from each peak center. The dynamic data were summed over time. For the lactate experiments, 3D MRSI data were reconstructed using the open source SIVIC package (27), and metabolite peak areas were loaded into OsiriX (28) as imaging data using a SIVIC function that generates quantitative images for each metabolite in 3D enhanced DICOM format. Mean tissue-

specific signals were isolated by manually drawing regions of interest (ROIs) on the anatomic ^{1}H imaging data, which were then automatically transferred to the ^{13}C images for computing ROI statistics by means of built-in OsiriX functions, as shown in Figure 3. Because both fed and fasting studies were conducted in the same rats, fed and fasted metabolic profiles were compared by means of paired, two-tailed Student's t-tests, while diabetic profiles were compared with the normal fed state using the corresponding unpaired test. These tests, of course, rely on an implicit assumption that the data are normally distributed, which should reasonably describe experimental sources of error in our studies.

Measurement of PEPCK Expression Levels

Phosphoenolpyruvate carboxykinase (PEPCK) is considered to be the rate-limiting enzyme of gluconeogenesis, and PEPCK expression is a widely used marker of gluconeogenesis (29). We measured expression levels of PEPCK in liver and kidney tissues of the seven STZ-treated rats and seven additional vehicle-treated controls, using quantitative polymerase chain reaction (PCR) analysis. Diabetic rats were treated with insulin until 36 h before organ harvesting. Liver and kidney RNA was prepared and analyzed using standard techniques (30). Rats were anesthetized with isoflurane and both kidneys and segments of liver were removed and flash frozen in liquid nitrogen and stored at −80°C; animals were then killed per protocol. Frozen whole kidney and liver sections were pulverized using mortar and pestle under liquid nitrogen followed by homogenization in Trizol using a Dounce homogenizer and phase separation with chloroform. Following centrifugation, the aqueous phase was removed and RNA was extracted using an RNeasy Mini kit (Qiagen, Hilden, Germany) with on-column DNase I digestion (Qiagen). cDNA was then generated using iScript cDNA synthesis kit (Bio-Rad, Hercules, CA). Quantitative real-time PCR was performed using the StepOnePlus system (Thermo Fisher, Watham, MA) with iTaq Universal SYBR Green master mix (Bio-Rad). The values for PEPCK expression levels were calculated by comparative C_T method with normalization to β-actin (31).

RESULTS

Multiple sets of notable metabolic modulations were detected in association with fasting and STZ diabetes, as described in the following sections. To reduce potential variation between experiments due to level of polarization, concentration and volume of infusion, and tissue perfusion, among other factors, we report metabolite ratios as opposed to the raw metabolite signals.

Effect of Fasting

Metabolite profiles of the HP pyruvate, lactate, alanine, and bicarbonate resonances (e.g. as depicted in Figure 4) were investigated. Inspection revealed that fasting resulted in three main modulations of these profiles in comparison with the normal fed (control) condition. First, in fasting, the ratio of HP bicarbonate signal to total ^{13}C signal was lower than control by 52% and 46% in liver and kidney slabs, respectively ($P = 0.004, 0.012$; see Figure 4 for representative spectra, and Figure 6 for summary quantitative data). Second, in fasting, the ratio of HP alanine signal to total ^{13}C signal was lower by 13% and 12% in liver and kidney slabs, respectively ($P = 0.001, 0.013$). These first two results were derived from the

experiments with pyruvate as the primary HP substrate. Third, in fasting, the ratio of HP lactate to alanine was 54% higher specifically in the liver ($P = 0.019$), but no significant effect in kidney was observed. This third result was obtained with lactate as the primary HP substrate. Except for sporadic detection of a very small additional resonance just upfield from [1-^{13}C]alanine, probably [1-^{13}C]aspartate (Figure 4, lower right panel), no signals in addition to the peaks labeled in the top left panel of Figure 4 were reproducibly detected. The appearance of this peak was not correlated with fasting.

Effect of STZ Diabetes

The HP metabolite profile of insulin-deprived STZ diabetes generally resembled a more pronounced version of fasting with some interesting exceptions. First, in STZ diabetes as compared with the normal fed condition, the ratio of HP bicarbonate to total ^{13}C signal was lower by 38% and 49% in liver and kidney slabs, respectively ($P = 0.060$, 0.0061; data quantified below in Figure 6). Of interest, the magnitude of the reduction of the hepatic bicarbonate signal was actually smaller in diabetes than fasting, and unlike kidney, did not meet statistical significance in this study. A potential explanation for this effect related to the extraordinarily high level of GCN in the STZ diabetic state is discussed below. Second, for the same comparison of STZ diabetes as compared with the normal fed condition, the ratio of HP alanine to total ^{13}C signal was also lower by 26% and 30% in liver and kidney slabs, respectively ($P = 0.007$, 0.005). These first two results were again derived from experiments with HP pyruvate as the primary substrate.

Third, for the same comparison of STZ diabetes as compared with the normal fed condition, the ratio of HP lactate-to-alanine was 69% higher in liver ($P = 0.007$), and 93% higher in the kidneys ($P = 0.004$). This result was obtained with HP lactate as the primary substrate. For a convincing display of this result, HP lactate-to-alanine metabolite ratio images from one STZ rat that was scanned in both baseline and post-STZ states is shown in Figure 5. Fourth, STZ diabetes additionally resulted in increased production of HP lactate from primary injected HP pyruvate in the kidney slab. The renal HP lactate-to-pyruvate ratio was elevated by 40% ($P = 0.047$). Full quantitative results from both the fasting and diabetes studies are summarized in Figure 6, which best illustrates the generally graded intensity of changes observed in fasting and diabetes.

PEPCK Expression Levels

As shown in Figure 7, PEPCK expression was found to be 5.86-fold higher in liver ($P = 0.0099$, unpaired t-test) and 2.73-fold greater in kidney ($P = 0.0324$, unpaired t-test) of STZ-treated rats as compared with vehicle.

DISCUSSION

Lactate and pyruvate are key metabolites involved in several important metabolic pathways, including a prominent role as glucose precursors in GCN. Previous investigations have suggested that the kidney is an important source of systemic glucose derived from GCN, particularly in prolonged fasting, and in diabetic states (1,5,32). However, progress in this area has been severely limited because studies have required highly invasive techniques,

with limited utility. The results of the present study demonstrate the feasibility of ^{13}C MRSI of HP gluconeogenic precursors for noninvasively tracking local alterations in the signals of selected key intermediates in glucose metabolism in response to fasting and diabetes, spatially resolved to the liver and kidneys. Organ-specific signal changes were detected with generally graded intensity from fasting to STZ-induced diabetes, particularly in the kidneys, consistent with the interpretation of diabetes as a “perceived” state of cellular starvation, and supporting a significant role for the kidneys in disease pathogenesis.

The changes in several of the MRSI signals could be interpreted as metabolic consequences of fasting and/or insulin deficiency. During fasting, high levels of acetyl-CoA due to breakdown of fatty acids potently inhibit PDC (33), potentially leading to the reduced ^{13}C-bicarbonate signal observed with fasting. Acetyl-coA likewise stimulates, and is in fact required for, carboxylation of pyruvate by pyruvate carboxylase (PC), the first committed step in GCN from the main precursors. Surprisingly, however, the hepatic bicarbonate signal partially rebounded in the diabetic rats relative to fasting, although the somewhat low SNR of the bicarbonate peak limits the certainty of this finding. Metabolic flux through phosphoenolpyruvate carboxykinase (PEPCK), thought to be a primary regulatory point of GCN, could theoretically also have yielded [^{13}C]bicarbonate signal.

Although cleavage of PEP occurs at the distal end of the carbon backbone from the C_1 label, the label could distribute symmetrically at both ends if conversion proceeds through fumarate (i.e., by means of interconversion with malate during shuttling of reducing equivalents), leading to the preliminary suggestion by an earlier report that [^{13}C]bicarbonate signal could actually mark GCN in a perfused liver system (15). A subsequent report mostly rejects the applicability of this suggestion in vivo, attributing the prior preliminary result to the octanoate content of the liver perfusate (34). Our data from a larger, in vivo fasting subject group likewise suggests that appearance of bicarbonate signal in vivo is, like in the heart, most likely tied primarily only to flux through PDC (14). Of interest, however, the partial rebound in diabetic rats could be due to the especially high PEPCK activity in this case.

Considering that lactate is the primary gluconeogenic precursor, and liver is the primary gluconeogenic organ in short-term fasting as performed in this study, the liver-specific elevation of HP lactate-to-alanine ratio (derived from HP lactate injections) in fasting may reflect the expected local bulk metabolic shift in glucose metabolism toward glucose formation. Multiple studies support a smaller but still significant role for renal GCN even in short-term fasting conditions similar to our study. Studies in dogs and humans have shown that overnight fasting results in a ~30% contribution of renal GCN to total GCN (35,36). This could account for the detected effect of fasting on renal HP alanine signal (in the case of HP pyruvate injections). The renal component of GCN is expected to rise very substantially during a longer fast, or diabetic and/or acidotic conditions. The detected modulations were, in fact, magnified and fully expanded to the kidneys in the diabetic state.

The PEPCK expression data obtained in STZ-treated rats in this study support a significant elevation of renal gluconeogenesis in addition to its hepatic counterpart in diabetes. There are several possible explanations for the reduced HP alanine signal level observed during

fasting, which has also been observed previously in the liver under similar experimental conditions, with similar magnitude (37). One possible mechanism is increased usage of alanine as a gluconeogenic precursor during fasting (i.e. a shift of the glucose-alanine cycle toward glucose production), due to changes in ALT and/or downstream enzymes resulting in the observed reduction of alanine levels.

However, comparable reductions were observed for both liver and kidney in the case of the HP pyruvate studies, although only the liver would be expected to use alanine significantly. Under normal conditions, renal usage of alanine is only approximately 10% relative to lactate (38). Another possible explanation is enhanced competition of aspartate transaminase with ALT for glutamate during fasting. GCN from lactate relies largely on transamination of oxaloacetate with glutamate to transfer its carbon backbone to the cytosol for further steps in GCN. Such an effect could theoretically explain the larger effect on alanine levels observed in the HP lactate experiments.

While we find these results extremely promising, the results should be interpreted with a few potentially significant limitations of the described approach in mind. Although based on prior HP imaging studies we expect the HP signals in the described liver and kidney slabs to be dominated by the respective organs, this gross type of localization is imperfect and does likely thus include some mixing of metabolism from adjacent tissues and the blood pool. This consideration only applied to the HP pyruvate data, which was acquired in this manner, but also complicates comparison with the HP lactate data, which was more fully localized.

Comparison of the results of injections of HP lactate and pyruvate is also complicated by the difference in the time points that were sampled, because the pyruvate data consisted of the summation of signals acquired over 60 s, while the lactate data consisted of only a single time frame acquired 30 s after the start of injection. The supraphysiologic levels of pyruvate used in this study are also a potential limitation, but this is not a major concern as long as the data are interpreted correctly. This limitation can be addressed by the use of lactate injection. A potential complication of our fed versus fasted study protocol is an inability to precisely control the “fed” condition. While the fasted condition is well-controlled, the “fed” rats could have substantial variation in the time elapsed since the last meal. Considering that scans were conducted in the afternoon although rats typically feed at night, some of the “fed” rats may actually have been fasting for a few hours. This issue could be addressed through gavage feeding.

In summary, viewed together, the lower levels of production of bicarbonate and alanine from HP glucose precursors in both liver and kidney in gluconeogenic states strongly suggest higher flux through the GCN pathway as compared with alternative metabolic fates. Thus the pattern of detectable intermediates of glucose metabolism derived from HP ^{13}C lactate and/or pyruvate could help define a metabolic signature of GCN which could be extremely valuable for preclinical and ultimately perhaps clinical studies of the differential regulation of hepatic and renal components of GCN in diabetes. The observed elevated production of lactate in the kidney in diabetes on the other hand strongly suggests localized activation of LDH and alteration of the normal renal cytoplasmic redox state, probably resulting from hyperglycemia by means of activation of the polyol pathway (39). This finding is in

agreement with the results of a prior initial renal HP ^{13}C MR study of STZ-induced diabetes (40).

CONCLUSIONS

The intermediary metabolism of gluconeogenic precursors [1-^{13}C]lactate and [1-^{13}C]pyruvate can be monitored noninvasively in vivo using HP ^{13}C MRSI. Localized changes in the HP metabolic spectra of these probes in the liver and kidneys were detected in states of increasing GCN activity, with generally graded intensity of response from fasting to diabetes. These HP ^{13}C methods could be extremely useful for noninvasive monitoring of hepatic and renal components of GCN in future preclinical and ultimately clinical studies.

ACKNOWLEDGEMENTS

We gratefully acknowledge grant funding support from NIH K01DK099451, P41EB013598, and R01DK056695. We also acknowledge support from a gift from the James Hilton Manning and Emma Austin Manning Foundation (DP), as well as support from NIH T32DK007219 and the Ben J Lipps Fellowship of the American Society of Nephrology (GYC).

REFERENCES

1. Meyer C, Stumvoll M, Nadkarni V, Dostou J, Mitrakou A, Gerich J. Abnormal renal and hepatic glucose metabolism in type 2 diabetes mellitus. J Clin Invest. 1998; 102:619–624. [PubMed: 9691098]
2. Devlin, TM. Textbook of biochemistry with clinical correlations. Wiley-Liss; New York: 2002.
3. Gladden LB. Lactate metabolism: a new paradigm for the third millennium. J Physiol (Lond). 2004; 558:5–30. [PubMed: 15131240]
4. Exton JH, Park CR. Control of gluconeogenesis in liver. I. General features of gluconeogenesis in the perfused livers of rats. J Biol Chem. 1967; 242:2622–2636. [PubMed: 6027238]
5. Gerich JE, Meyer C, Woerle HJ, Stumvoll M. Renal gluconeogenesis - its importance in human glucose homeostasis. Diabetes Care. 2001; 24:382–391. [PubMed: 11213896]
6. Landau BR, Wahren J, Chandramouli V, Schumann WC, Ekberg K, Kalhan SC. Use of 2H2O for estimating rates of gluconeogenesis. Application to the fasted state. J Clin Invest. 1995; 95:172–178. [PubMed: 7814612]
7. Stumvoll M, Meyer C, Perriello G, Kreider M, Welle S, Gerich J. Human kidney and liver gluconeogenesis: evidence for organ substrate selectivity. Am J Physiol Endocrinol Metab. 1998; 274:E817–E826.
8. Ardenkjaer-Larsen JH, Fridlund B, Gram A, Hansson G, Hansson L, Lerche MH, Servin R, Thaning M, Golman K. Increase in signal-to-noise ratio of > 10,000 times in liquid-state NMR. Proc Natl Acad Sci U S A. 2003; 100:10158–10163. [PubMed: 12930897]
9. Golman K, in ’t Zandt R, Thaning M. Real-time metabolic imaging. Proc Natl Acad Sci U S A. 2006; 103:11270–11275. [PubMed: 16837573]
10. Nelson SJ, Kurhanewicz J, Vigneron DB, et al. Metabolic imaging of patients with prostate cancer using hyperpolarized [1-^{13}C]pyruvate. Sci Transl Med. 2013; 5:198ra108.
11. Chen AP, Kurhanewicz J, Bok R, Xu D, Joun D, Zhang V, Nelson SJ, Hurd RE, Vigneron DB. Feasibility of using hyperpolarized[1-13C]lactate as a substrate for in vivo metabolic 13C MRSI studies. Magn Reson Imaging. 2008; 26:721–726. [PubMed: 18479878]
12. Chen AP, Lau JYC, Alvares RDA, Cunningham CH. Using [1-(13) C]lactic acid for hyperpolarized (13) C MR cardiac studies. Magn Reson Med. 2014 doi: 10.1002/mrm.25354.
13. Albers MJ, Bok R, Chen AP, et al. Hyperpolarized 13C lactate, pyruvate, and alanine: noninvasive biomarkers for prostate cancer detection and grading. Cancer Res. 2008; 68:8607–8615. [PubMed: 18922937]

14. Schroeder MA, Cochlin LE, Heather LC, Clarke K, Radda GK, Tyler DJ. In vivo assessment of pyruvate dehydrogenase flux in the heart using hyperpolarized carbon-13 magnetic resonance. Proc Natl Acad Sci U S A. 2008; 105:12051–12056. [PubMed: 18689683]
15. Merritt ME, Harrison C, Sherry AD, Malloy CR, Burgess SC. Flux through hepatic pyruvate carboxylase and phosphoenolpyruvate carboxykinase detected by hyperpolarized 13C magnetic resonance. Proc Natl Acad Sci U S A. 2011; 108:19084–19089. [PubMed: 22065779]
16. Hu S, Balakrishnan A, Bok RA, Anderton B, Larson PEZ, Nelson SJ, Kurhanewicz J, Vigneron DB, Goga A. 13C-pyruvate imaging reveals alterations in glycolysis that precede c-Myc-induced tumor formation and regression. Cell Metab. 2011; 14:131–142. [PubMed: 21723511]
17. Day SE, Kettunen MI, Gallagher FA, Hu D-E, Lerche M, Wolber J, Golman K, Ardenkjaer-Larsen JH, Brindle KM. Detecting tumor response to treatment using hyperpolarized 13C magnetic resonance imaging and spectroscopy. Nat Med. 2007; 13:1382–1387. [PubMed: 17965722]
18. Hurd RE, Spielman D, Josan S, Yen Y-F, Pfefferbaum A, Mayer D. Exchange-linked dissolution agents in dissolution-DNP (13)C metabolic imaging. Magn Reson Med. 2013; 70:936–942. [PubMed: 23165935]
19. Jin ES, Moreno KX, Wang J-X, Fidelino L, Merritt ME, Sherry AD, Malloy CR. Metabolism of hyperpolarized [1-13C]pyruvate through alternate pathways in rat liver. NMR in Biomedicine. 2016:466–474. [PubMed: 26836042]
20. Palm F, Ortsater H, Hansell P, Liss P, Carlsson PO. Differentiating between effects of streptozotocin per se and subsequent hyperglycemia on renal function and metabolism in the streptozotocin-diabetic rat model. Diabetes Metab Res Rev. 2004; 20:452–459. [PubMed: 15386825]
21. Cunningham CH, Chen AP, Albers MJ, Kurhanewicz J, Hurd RE, Yen Y-F, Pauly JM, Nelson SJ, Vigneron DB. Double spin-echo sequence for rapid spectroscopic imaging of hyperpolarized 13C. J Magn Reson. 2007; 187:357–362. [PubMed: 17562376]
22. Zhao L, Mulkern R, Tseng CH, Williamson D, Patz S, Kraft R, Walsworth RL, Jolesz FA, Albert MS. Gradient-echo imaging considerations for hyperpolarized 129Xe MR. J Magn Reson B. 1996; 113:179–183.
23. von Morze, C., Larson, PEZ., Shang, H., Vigneron, DB. Suppression of unwanted resonances in hyperpolarized MR studies with neat [1-13C]lactic acid; Proceedings of the 22nd Annual Meeting of ISMRM; Milan, Italy. 2014; Abstract 2792
24. Pauly J, Le Roux P, Nishimura D, Macovski A. Parameter relations for the Shinnar-Le Roux selective excitation pulse design algorithm [NMR imaging]. IEEE Trans Med Imaging. 1991; 10:53–65. [PubMed: 18222800]
25. von Morze C, Larson PEZ, Hu S, Yoshihara HAI, Bok RA, Goga A, Ardenkjaer-Larsen JH, Vigneron DB. Investigating tumor perfusion and metabolism using multiple hyperpolarized 13C compounds: HP001, pyruvate and urea. Magn Reson Imaging. 2012; 30:305–311. [PubMed: 22169407]
26. Lee P, Leong W, Tan T, Lim M, Han W, Radda GK. In vivo hyperpolarized carbon-13 magnetic resonance spectroscopy reveals increased pyruvate carboxylase flux in an insulin-resistant mouse model. Hepatology. 2013; 57:515–524. [PubMed: 22911492]
27. Crane JC, Olson MP, Nelson SJ. SIVIC: open-source, standards-based software for DICOM MR spectroscopy workflows. Int J Biomed Imaging. 2013; 2013:169526–169512. [PubMed: 23970895]
28. Rosset A, Spadola L, Ratib O. OsiriX: an open-source software for navigating in multidimensional DICOM images. J Digit Imaging. 2004; 17:205–216. [PubMed: 15534753]
29. Chakravarty K, Cassuto H, Reshef L, Hanson RW. Factors that control the tissue-specific transcription of the gene for phosphoenolpyruvate carboxykinase-C. Crit Rev Biochem Mol Biol. 2005; 40:129–154. [PubMed: 15917397]
30. Soundararajan R, Zhang TT, Wang J, Vandewalle A, Pearce D. A novel role for glucocorticoid-induced leucine zipper protein in epithelial sodium channel-mediated sodium transport. J Biol Chem. 2005; 280:39970–39981. [PubMed: 16216878]
31. Schmittgen TD, Livak KJ. Analyzing real-time PCR data by the comparative C-T method. Nat Protoc. 2008; 3:1101–1108. [PubMed: 18546601]

32. Mitrakou A. Kidney: its impact on glucose homeostasis and hormonal regulation. Diabetes Res Clin Pract. 2011; 93:S66–S72. [PubMed: 21864754]
33. Holness MJ, Sugden MC. Pyruvate-dehydrogenase activities during the fed-to-starved transition and on re-feeding after acute or prolonged starvation. Biochem J. 1989; 258:529–533. [PubMed: 2705997]
34. Moreno KX, Moore CL, Burgess SC, Sherry AD, Malloy CR, Merritt ME. Production of hyperpolarized 13CO2 from [1-13C]pyruvate in perfused liver does reflect total anaplerosis but is not a reliable biomarker of glucose production. Metabolomics. 2015:1–13.
35. Cersosimo E, Judd RL, Miles JM. Insulin regulation of renal glucose metabolism in conscious dogs. J Clin Invest. 1994; 93:2584–2589. [PubMed: 8200996]
36. Stumvoll M, Chintalapudi U, Perriello G, Welle S, Gutierrez O, Gerich J. Uptake and release of glucose by the human kidney. Postabsorptive rates and responses to epinephrine. J Clin Invest. 1995; 96:2528–2533. [PubMed: 7593645]
37. Hu S, Chen AP, Zierhut ML, Bok R, Yen Y-F, Schroeder MA, Hurd RE, Nelson SJ, Kurhanewicz J, Vigneron DB. In vivo carbon-13 dynamic MRS and MRSI of normal and fasted rat liver with hyperpolarized 13C-pyruvate. Mol Imaging Biol. 2009; 11:399–407. [PubMed: 19424761]
38. Meyer C, Stumvoll M, Dostou J, Welle S, Haymond M, Gerich J. Renal substrate exchange and gluconeogenesis in normal postabsorptive humans. Am J Physiol Endocrinol Metab. 2002; 282:E428–E434. [PubMed: 11788376]
39. Nordquist L, Palm F. Diabetes-induced alterations in renal medullary microcirculation and metabolism. Curr Diabetes Rev. 2007; 3:53–65. [PubMed: 18220656]
40. Laustsen C, Østergaard JA, Lauritzen MH, Nørregaard R, Bowen S, Søgaard LV, Flyvbjerg A, Pedersen M, Ardenkjaer-Larsen JH. Assessment of early diabetic renal changes with hyperpolarized [1-13C]pyruvate. Diabetes Metab Res Rev. 2013; 29:125–129. [PubMed: 23166087]

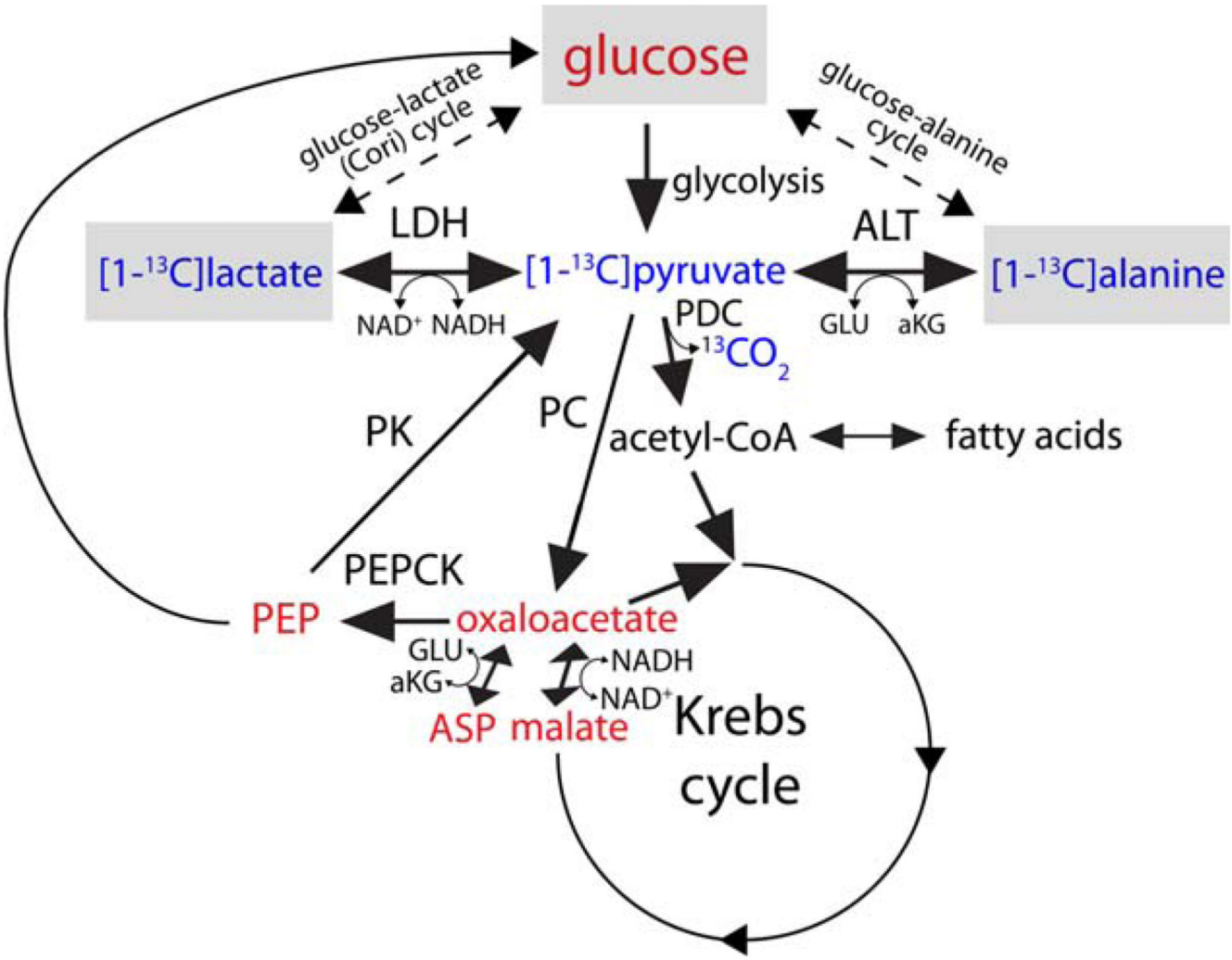

FIG. 1.

Primary pathways of glucose recycling, glucose-lactate (Cori) and glucose-alanine cycles. The three dominant mobilized metabolites are shown in gray boxes. Potential molecular fates of ^{13}C label originating at C_1 of lactate or pyruvate are indicated in color, with intermediates routinely observable by means of HP ^{13}C MRSI in blue, and typically invisible fates in red. LDH, lactate dehydrogenase; PDC, pyruvate dehydrogenase complex; ALT, alanine transaminase; PC, pyruvate carboxylase; PK, pyruvate kinase; GLU, glutamate; aKG, alpha-ketoglutarate; ASP, aspartate; PEP, phosphoenolpyruvate.

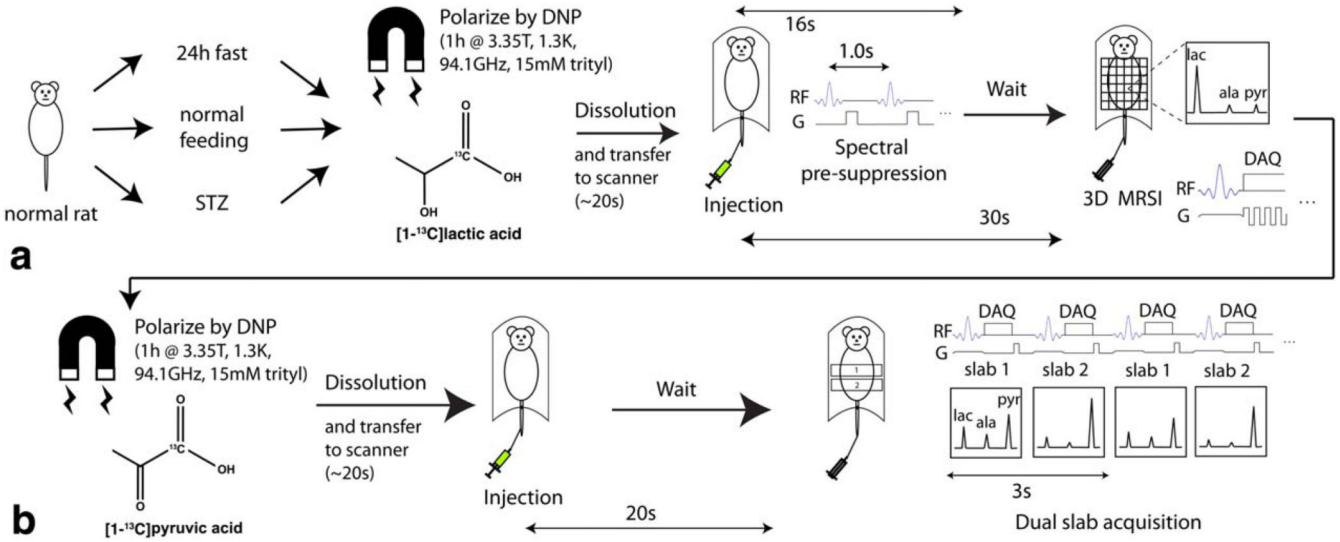

FIG. 2.

Graphical summary of methods for HP ^{13}C MR experiments with ^{13}C-lactate (**A**) and ^{13}C-pyruvate (**B**). Each experiment consisted of both scans run successively in a single session. Each polarization buildup lasted ~1 h, followed by rapid dissolution and transfer to the MRI scanner, followed by intravenous injection into the rat and rapid data acquisition.

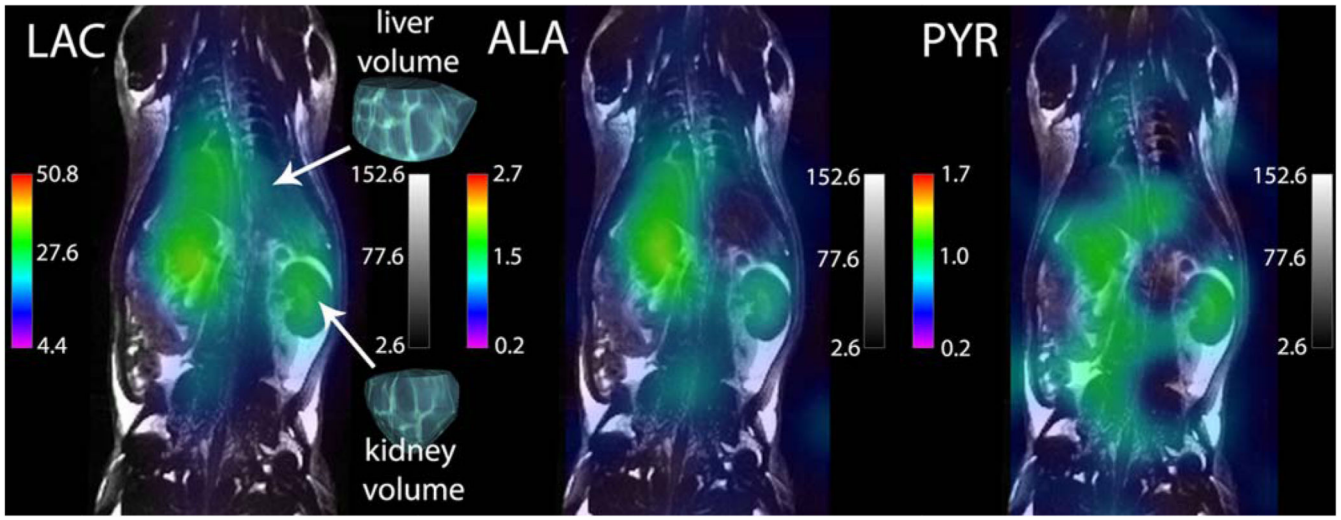

FIG. 3.

Coronal MRSI of HP [1-^{13}C]lactate in fed rat. Localized spectra were integrated to produce 3D metabolite images (color) of lactate and HP products alanine and pyruvate, shown overlaid on ^{1}H SSFP anatomic images (grayscale) using OsiriX. Volume renderings of 3D liver and kidney ROIs generated in OsiriX for data analysis are also shown.

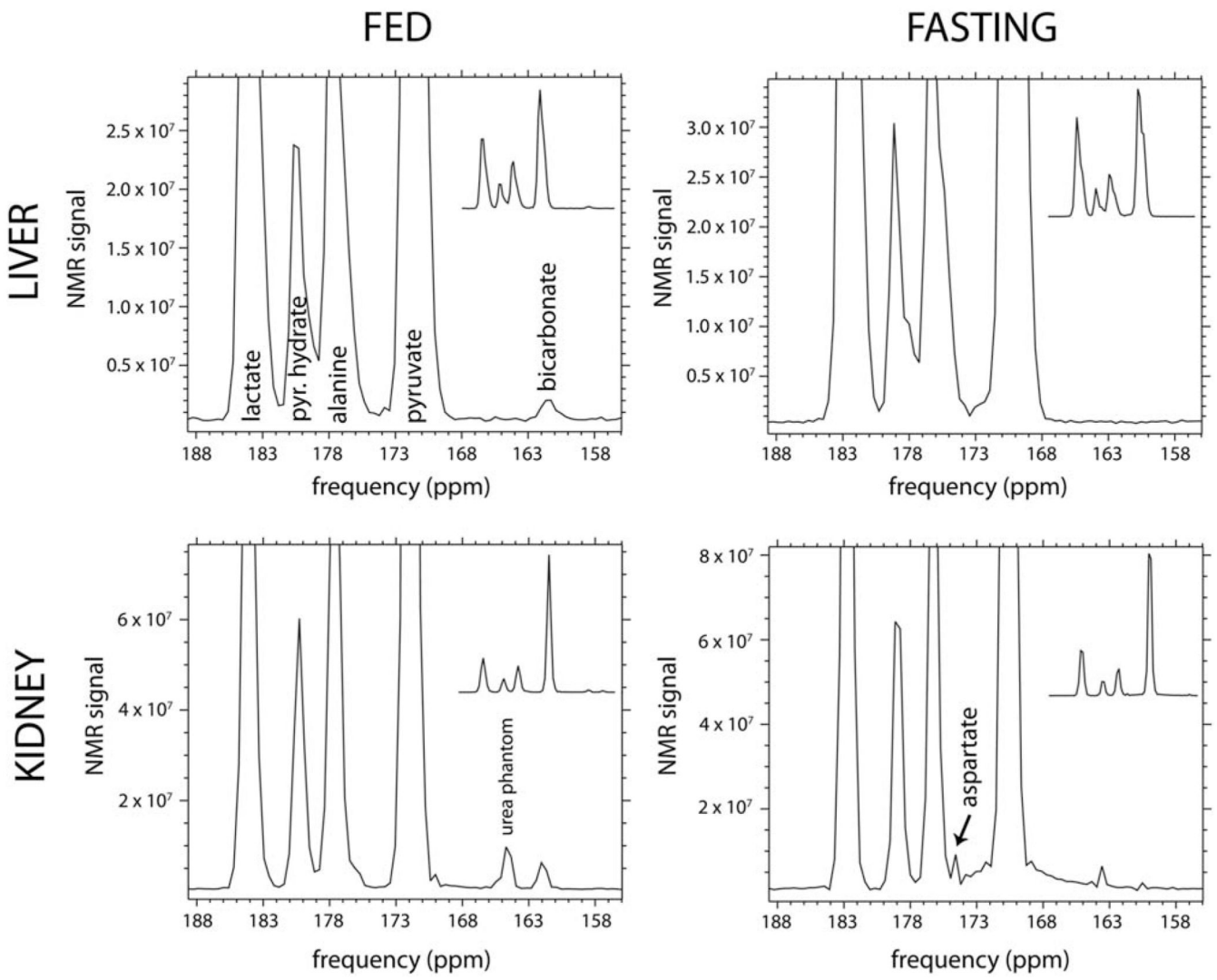

FIG. 4.

In vivo HP ^{13}C MR spectra obtained from liver (top row) and kidney (bottom row) slabs of a representative normal rat following injections of HP ^{13}C-pyruvate, in both normal fed (left column) and fasting (right column) states. These spectra clearly depict the large reduction of ^{13}C-bicarbonate signal detected in both organs with fasting. Spectra are zoomed to show the ^{13}C-bicarbonate peak. Corresponding unzoomed spectra are also included as insets in each figure panel for reference. NMR signal magnitude is shown, by convention.

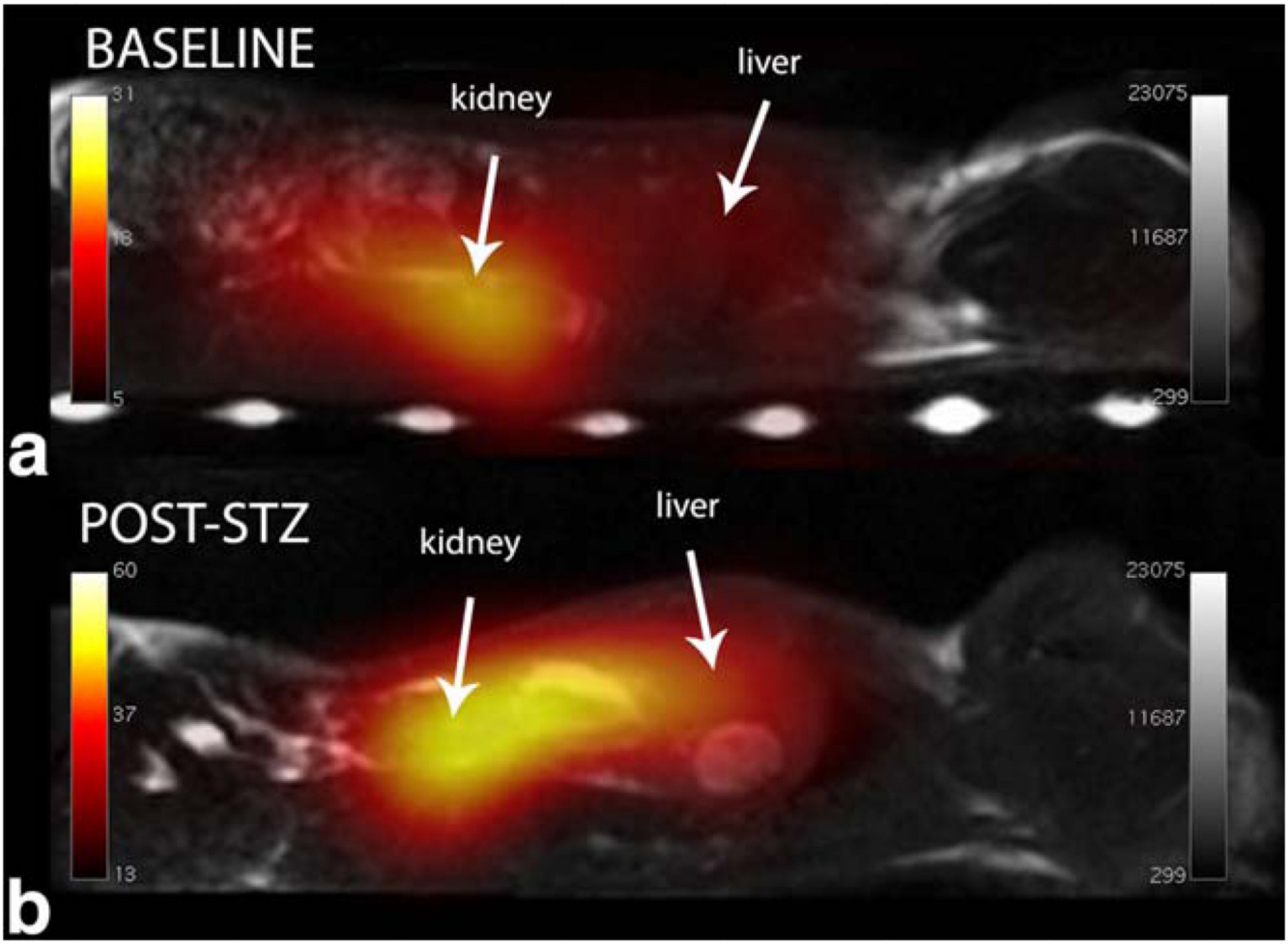

FIG. 5.

Sagittal images of HP ^{13}C lactate-to-alanine ratio (color) overlaid on standard ^{1}H images (grayscale), in baseline and post-STZ states. Lactate-to-alanine ratio increased by 61% in liver and 140% in kidney after STZ in this case.

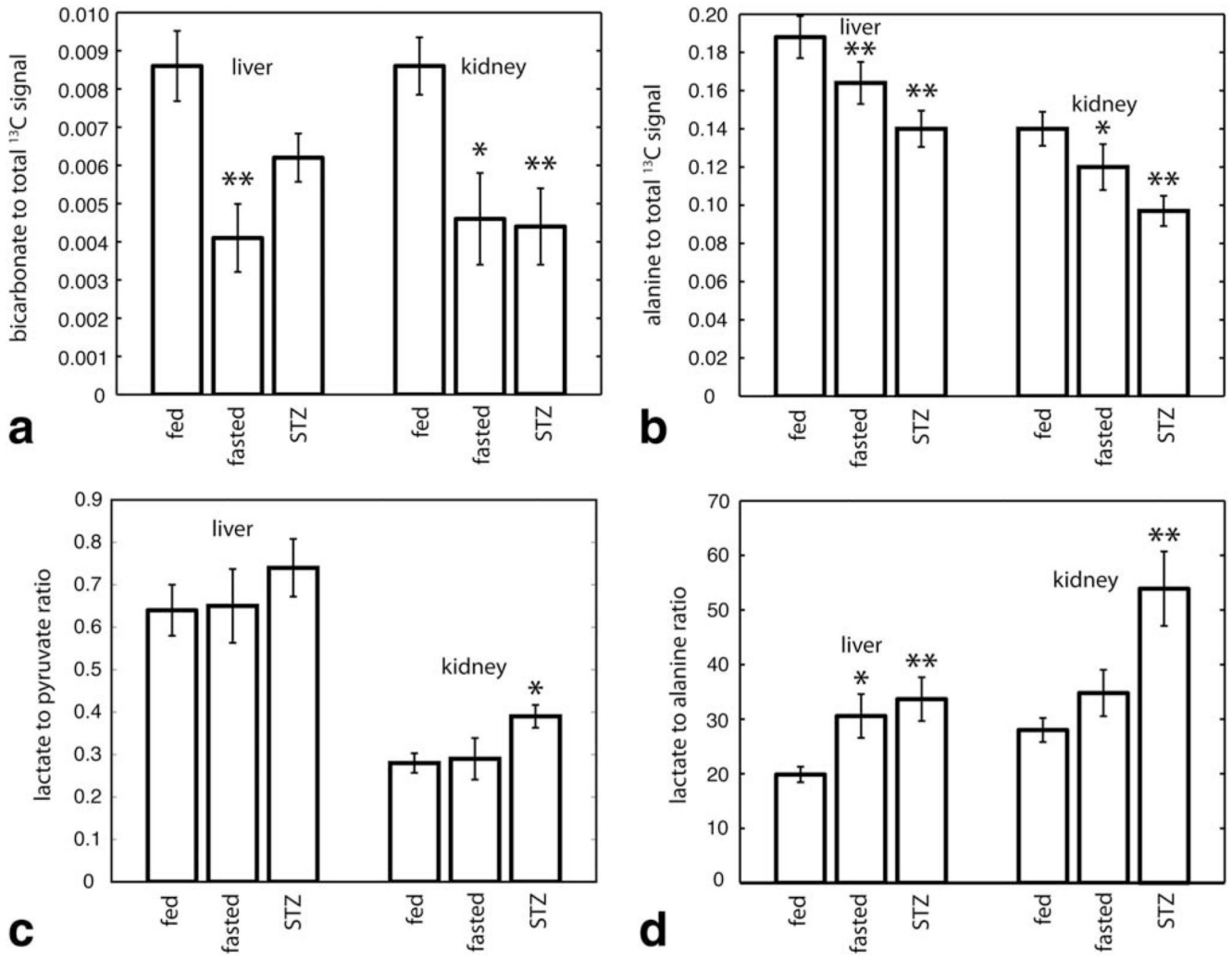

FIG. 6.

Bar graphs summarizing key local effects of fasting and STZ diabetes on HP metabolite ratios for HP pyruvate (**A–C**) and lactate (**D**) experiments (*0.01 < P < 0.05; **P < 0.01). See text for details. Error bars represent standard error of the mean.

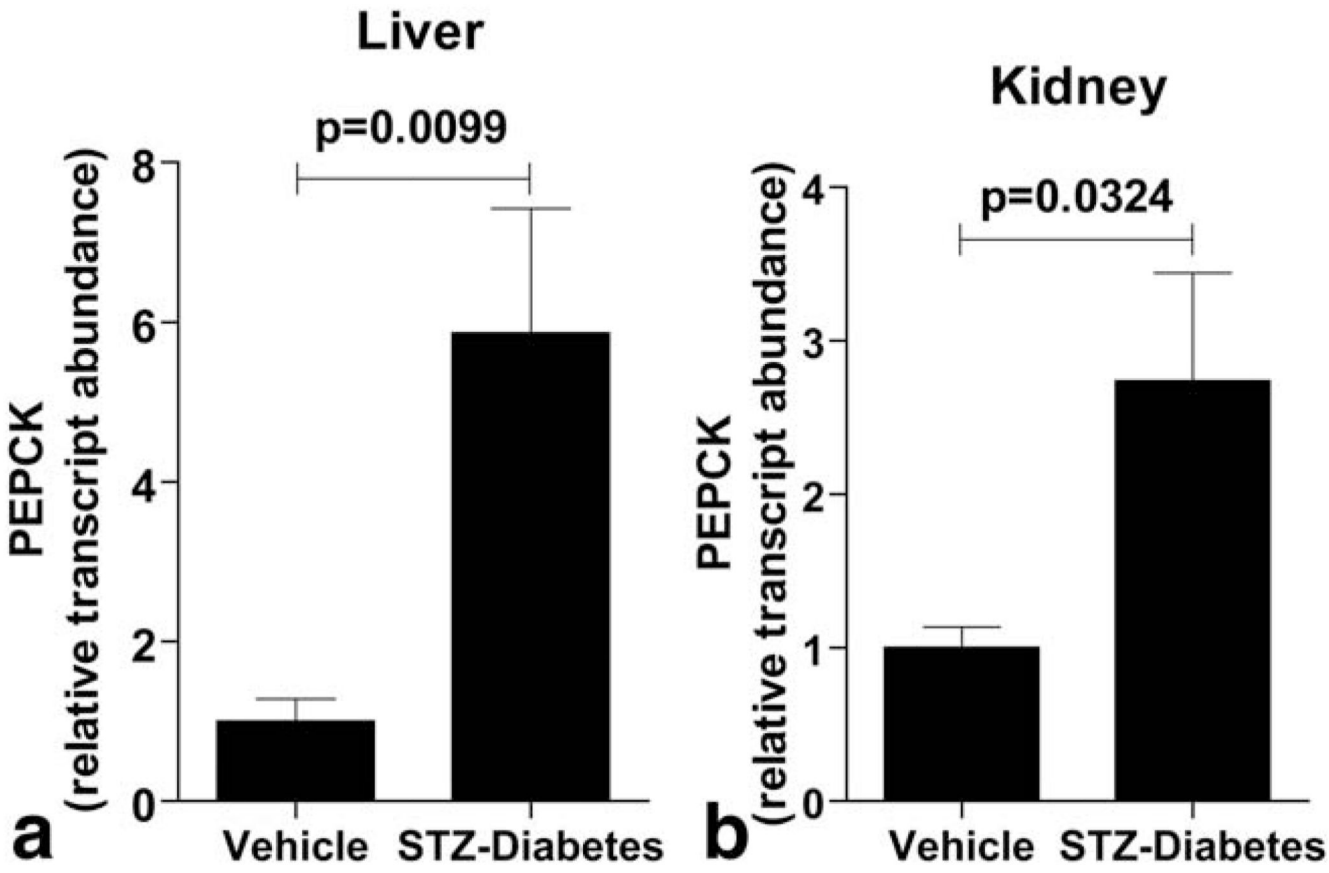

FIG. 7.

Bar graphs showing PEPCK expression levels in STZ-treated diabetic animals relative to vehicle-treated controls. PEPCK is markedly increased in both liver (**A**) and kidney (**B**) of STZ-treated diabetic rats. Real-time PCR was repeated three times and the data shown is the average of all three experiments.